Available online at www.sciencedirect.com
SCIENCE DIRECT®
Journal of Computational Physics 190 (2003) 398–418
JOURNAL OF COMPUTATIONAL PHYSICS
www.elsevier.com/locate/jcp

Exact boundary condition for time-dependent wave equation based on boundary integral

Zhen-Huan Teng [1]

LMAM and School of Mathematical Sciences, Peking University, Beijing 100871, China

Received 11 September 2002; received in revised form 28 April 2003; accepted 21 May 2003

Abstract

An exact non-reflecting boundary conditions based on a boundary integral equation or a modified Kirchhoff-type formula is derived for exterior three-dimensional wave equations. The Kirchhoff-type non-reflecting boundary condition is originally proposed by L. Ting and M.J. Miksis [J. Acoust. Soc. Am. 80 (1986) 1825] and numerically tested by D. Givoli and D. Cohen [J. Comput. Phys. 117 (1995) 102] for a spherically symmetric problem. The computational advantage of Ting–Miksis boundary condition is that its temporal non-locality is limited to a fixed amount of past information. However, a long-time instability is exhibited in testing numerical solutions by using a standard non-dissipative finite-difference scheme. The main purpose of this work is to present a new exact boundary condition and to eliminate the long-time instability. The proposed exact boundary condition can be considered as a limit case of Ting–Miksis boundary condition when the two artificial boundaries used in their method approach each other. Our boundary condition is actually a boundary integral equation on a single artificial boundary for wave equations, which is to be solved in conjunction with the interior wave equation. The new boundary condition needs only one artificial boundary, which can be of any shape, i.e., sphere, cubic surface, etc. It keeps all merits of the original Kirchhoff boundary condition such as restricting the temporal non-locality, free of numerical evaluation of any special functions and so on. Numerical approximation to the artificial boundary condition on cubic surface is derived and three-dimensional numerical tests are carried out on the cubic computational domain.

Keywords: Wave equation; Non-reflecting boundary condition; Unbounded domain; Numerical methods; Artificial boundary condition; Boundary integral equation

1. Introduction

We consider the three-dimensional wave equation:

$$\frac{\partial^2 u}{\partial t^2} = c^2 \nabla^2 u + f(\boldsymbol{x}; t) \quad \text{in } \Omega \times (0, T), \tag{1}$$

E-mail address: tengzh@math.pku.edu.cn.
[1] Supported by the Special Funds for Major State Basic Research Projects of China.

0021-9991/$ - see front matter © 2003 Elsevier Science B.V. All rights reserved.
doi:10.1016/S0021-9991(03)00281-X

$$u = g \quad \text{or} \quad \partial_n u = g \quad \text{on } \gamma \times (0, T), \tag{2}$$

$$u(\boldsymbol{x}, 0) = u_0(\boldsymbol{x}) \quad \text{in } \Omega, \tag{3}$$

$$\partial_t u(\boldsymbol{x}, 0) = u_1(\boldsymbol{x}) \quad \text{in } \Omega, \tag{4}$$

where Ω is an infinite domain in three-dimension exterior to an obstacle or a scatterer with a boundary γ as indicated in Fig. 1, $u_0(\cdot)$, $u_1(\cdot)$ and $f(\cdot; t)$ have compact supports in $\boldsymbol{R}^3$.

In order to solve the problem numerically on unbounded domain by using a finite difference (FD) or a finite element (FE) method, one has to truncate the infinite domain via an artificial boundary $\mathscr{S}$ around the obstacle (see Fig. 2) and applying some boundary condition on $\mathscr{S}$, which is called artificial boundary condition or non-reflecting boundary condition (NRBC); see [1,3–5,8–10,14] for wave equation and [6,18] for recent review on this subject. An alternative way to handle the unbounded domain is to use spectral method with approximate basis functions, see, e.g. [12,15]. In this work, we will be interested in using artificial boundary conditions. The computational domain Ω_{i} is bounded internally by γ and externally by $\mathscr{S}$. The artificial boundary $\mathscr{S}$ is chosen to enclose all the "irregularities" in the unbounded domain. Here the "irregularities" means wave sources, non-zero initial conditions, inhomogeneous medium and so on. The unbounded domain exterior to $\mathscr{S}$ is denoted by Ω_{e}, which includes only zero initial conditions, homogeneous medium and no wave sources and where the medium is to be at rest for times $t \leqslant 0$.

In this paper, we derive a new exact NRBC for exterior three-dimensional wave equations by using a boundary integral equation or a modified Kirchhoff formula. The Kirchhoff-type NRBC is originally proposed by Ting and Miksis [17] and numerically tested by Givoli and Cohen [8] for one-dimensional problems. The computational advantage of this approach is that its temporal non-locality is limited to a fixed amount of past information. However, a long-time instability is exhibited in the testing numerical solutions by using a standard non-dissipative finite-difference scheme in the computational domain. This instability could be eliminated by introducing additional dissipation into the scheme as suggested in [8], but it is known that the central non-dissipative difference scheme for nonlinear wave equation is an *multi-symplectic* scheme [13], which has the advantage for computing long time evolution problem such as superior energy-conserving behavior, better preserving waveform and superior stability.

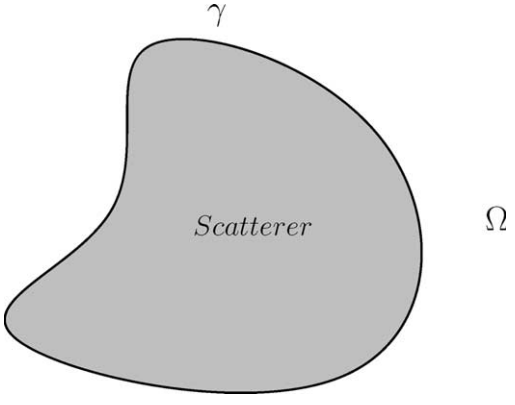

Fig. 1. The infinite domain Ω with a boundary γ.

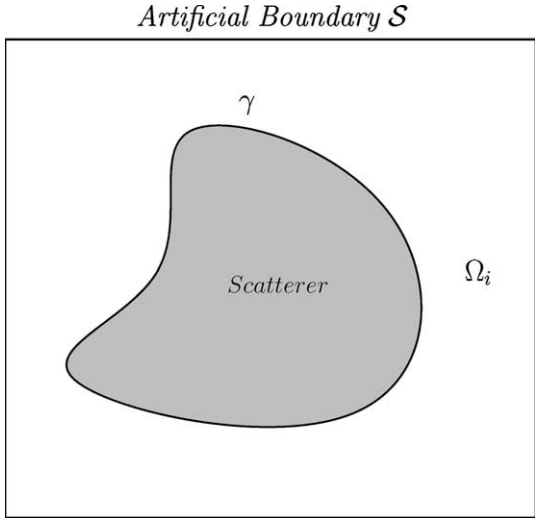

Fig. 2. $\mathscr{S}$ is an artificial boundary and Ω_i is computational domain.

The new NRBC proposed in this paper can be considered as a limit case of Ting–Miksis boundary condition when the two artificial boundaries used in their method approach each other. In fact, the limit boundary condition is a boundary integral equation on a single artificial boundary for wave equation. Since the boundary integral equation involves both u and $\partial_n u$ on the boundary, the boundary integral can not be solved independently and has to be solved in conjunction with the interior wave equation, which may has variable coefficients or is nonlinear. Therefore, the boundary integral equation can be considered as an exact artificial boundary condition for the interior wave equation. If the interior equation is discretized by FD or FE method and the boundary integral equation is approximated by quadrature formula (QF) or boundary element (BI) method, this is also called *coupled FD* or *FE with QF* or *BE method* for solving wave equation in infinite domains. In fact, the coupled FE with BE method for solving elliptic equation in unbounded domain is very popular and efficient (see e.g. [7]). As far as I know the work presented in this paper is the first to directly apply the boundary integral equation on a single artificial surface enclosing the scattering object and the wave equation with variable coefficient and to implement coupled FD in the resulting bounded domain problem with QF method for the boundary integral. Of course, the NRBC can also be implemented by using FE method in the interior domain and BE method on the boundary. This is an interesting research subject and will be reported elsewhere. It is noticed that a different approach is introduced in [14] to construct an artificial boundary condition with restricted temporal non-locality, which does not require a discrete approximation of the Kirchhoff integral.

It is shown that for the spherically symmetric case both continue version and discrete version of the new NRBC are equivalent to that of the local NRBC proposed by Engquist and Majda [4]. Numerical results obtained by using our NRBC for the one-dimensional problems verify our theoretical claims and demonstrate the desired long time stability.

The new NRBC only needs one artificial boundary, which is contrast to the original Kirchhoff-type condition which requires two artificial boundaries. The new boundary condition preserves the main advantages of Kirchhoff condition: the artificial boundary can be of any shape, i.e. sphere, cubic surface and so on; it requires only fixed storage of the past information of the solution at the artificial boundary; there is no need of any numerical evaluation of special functions; the size of the computation domain is of the same order as the scatterer; if explicit difference scheme is used in the interior domain, the

boundary condition can be solved at each time step independently, due to the retarded time property; for cubic artificial boundary only one set of mesh grid to both inside of and on boundary of the cube is required.

A key ingredient in deriving the new NRBC is the boundary integral equation or the modified Kirchhoff formula for the time-dependent wave equation, which is also obtained by using Green's formula.

Numerical approximation to the artificial boundary condition on cubic surface is derived and three-dimensional numerical tests are carried out on a cubic computational domain by using the standard non-dissipative central difference scheme. The numerical solutions are in good agreement with exact solutions without producing spurious reflection from the artificial boundary. The overall scheme is shown to be stable in all our tests.

2. Boundary integral equation and new NRBC

2.1. Kirchhoff's formula and boundary integral equation for wave equation

Let D be a three-dimensional unbounded domain with piecewise smooth interior boundary ∂D, indicated in Fig. 3, and $w(\cdot,\tau)$ be smooth function with compact support in $\boldsymbol{R}^3$. It is easy to show that

$$v(w_{\tau\tau} - c^2\nabla^2 w) - w(v_{\tau\tau} - c^2\nabla^2 v) = \tilde{\nabla}\cdot\{-c^2 v\nabla w + c^2 w\nabla v, vw_\tau - wv_\tau\},$$

where $\tilde{\nabla} = \{\nabla_\xi, \partial_\tau\}$ is the space-time gradient vector. Integrating over the domain $D\times[0,t]$ we obtain the Green's formula:

$$\begin{aligned}
&\int\int\int\int_{D\times[0,t]} \{v(w_{\tau\tau} - c^2\nabla_\xi^2 w) - w(v_{\tau\tau} - c^2\nabla_\xi^2 v)\}\,\mathrm{d}\boldsymbol{\xi}\,\mathrm{d}\tau \\
&\quad = \int\int\int\int_{D\times[0,t]} \tilde{\nabla}\cdot\{-c^2 v\nabla_\xi w + c^2 w\nabla_\xi v, vw_\tau - wv_\tau\}\,\mathrm{d}\boldsymbol{\xi}\,\mathrm{d}\tau \\
&\quad = \int\int\int_{\partial D\times[0,t]} (-c^2 v\nabla_\xi w + c^2 w\nabla_\xi v)\cdot\boldsymbol{n}\,\mathrm{d}\sigma_\xi\,\mathrm{d}\tau + \int\int\int_D (vw_\tau - wv_\tau)\,\mathrm{d}\boldsymbol{\xi}\Big|_{\tau=0}^{\tau=t},
\end{aligned} \tag{5}$$

where $\mathrm{d}\boldsymbol{\xi} = \mathrm{d}\xi_1\,\mathrm{d}\xi_2\,\mathrm{d}\xi_3$, $\boldsymbol{n}$ is the unit normal to ∂D as indicated in Fig. 3. The last integral in the above equation is obtained by using the divergence theorem and the fact that $w(\boldsymbol{\xi},\tau)$ is zero for sufficiently large $|\boldsymbol{\xi}|$.

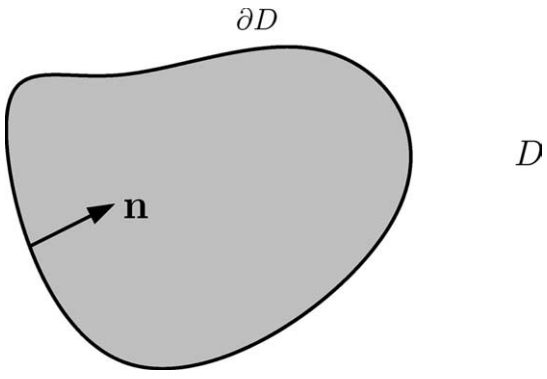

Fig. 3. The diagram for Green's formula.

Let $w(\boldsymbol{\xi},\tau)$ be a solution of the wave equation with compact initial data $w_0(\cdot)$ and $w_1(\cdot)$ in D, i.e.,

$$\begin{cases} \partial^2_{\tau\tau} w(\boldsymbol{\xi},\tau) - c^2\nabla^2_{\boldsymbol{\xi}} w(\boldsymbol{\xi},\tau) = 0, & (\boldsymbol{\xi},\tau) \in D \times R^+, \\ w|_{\tau=0} = w_0(\boldsymbol{\xi}),\ \partial_\tau w|_{\tau=0} = w_1(\boldsymbol{\xi}), & \boldsymbol{\xi} \in D, \end{cases}$$

where w and $\partial_{\boldsymbol{n}} w$ on the boundary ∂D are not prescribed, and v be the *fundamental* solution of the wave equation

$$v = \frac{1}{4\pi c|\boldsymbol{\xi}-\boldsymbol{x}|}\delta(c(\tau-t)+|\boldsymbol{\xi}-\boldsymbol{x}|),$$

where v satisfies $v_{\tau\tau} - c^2\nabla^2_{\boldsymbol{\xi}} v = \delta(\boldsymbol{\xi}-\boldsymbol{x})\delta(\tau-t)$ in the weak sense and $(\boldsymbol{x},t) \in D \times R^+$ is a given point. Then substituting w and v into the Green's formula (5) gives the Kirchhoff's formula (see [2,11]) with *non-zero initial data*:

$$\begin{aligned} w(\boldsymbol{x};t) = & -\frac{1}{4\pi}\int\int_{\partial D}\left([w]\frac{\partial}{\partial \boldsymbol{n}}\left(\frac{1}{\rho}\right) - \frac{1}{\rho}\left[\frac{\partial w}{\partial \boldsymbol{n}}\right] - \frac{1}{\rho c}\frac{\partial \rho}{\partial \boldsymbol{n}}\left[\frac{\partial w}{\partial t}\right]\right)\mathrm{d}\sigma_\xi \\ & + \frac{1}{4\pi(ct)^2}\int\int_{D\cap S(\boldsymbol{x},ct)}\left(w_0 - ct\frac{\partial w_0}{\partial \boldsymbol{n}} + tw_1\right)\mathrm{d}\sigma_\xi, \quad \boldsymbol{x} \in D, \end{aligned} \tag{6}$$

where $\rho = |\boldsymbol{\xi}-\boldsymbol{x}| = \sqrt{(\xi_1-x_1)^2+(\xi_2-x_2)^2+(\xi_3-x_3)^2}$, $S(\boldsymbol{x},R)$ is a spherical surface defined by $S(\boldsymbol{x},R) = \{\boldsymbol{\xi}\,|\,|\boldsymbol{\xi}-\boldsymbol{x}| = R\}$ and $\partial/\partial\boldsymbol{n}$ is the normal derivative at $\boldsymbol{\xi}$ on ∂D or $S(\boldsymbol{x},ct)$. The operator $[\cdot]$ above is the retarded value operator, defined by

$$[F] = F(\boldsymbol{\xi},\tau)|_{\tau=t-\rho/c}. \tag{7}$$

The derivation of the formula (6) requires some applications of the *generalized function* and we omit the details here (see for example [19]). By taking the limits of the above integral in the normal direction at ∂D as $\boldsymbol{x}$ approaching ∂D, we obtain the following *boundary integral equation* for the wave equation:

$$\begin{aligned} w(\boldsymbol{x};t) = & \frac{\Theta(\boldsymbol{x})}{4\pi}w(\boldsymbol{x};t) - \frac{1}{4\pi}\int\int_{\partial D}\left([w]\frac{\partial}{\partial \boldsymbol{n}}\left(\frac{1}{\rho}\right) - \frac{1}{\rho}\left[\frac{\partial w}{\partial \boldsymbol{n}}\right] - \frac{1}{\rho c}\frac{\partial \rho}{\partial \boldsymbol{n}}\left[\frac{\partial w}{\partial t}\right]\right)\mathrm{d}\sigma_\xi \\ & + \frac{1}{4\pi(ct)^2}\int\int_{D\cap S(\boldsymbol{x},ct)}\left(w_0 - ct\frac{\partial w_0}{\partial \boldsymbol{n}} + tw_1\right)\mathrm{d}\sigma_\xi, \quad \boldsymbol{x} \in \partial D, \end{aligned}$$

which is equivalent to

$$\begin{aligned} w(\boldsymbol{x};t)\left(1-\frac{\Theta(\boldsymbol{x})}{4\pi}\right) = & -\frac{1}{4\pi}\int\int_{\partial D}\left([w]\frac{\partial}{\partial \boldsymbol{n}}\left(\frac{1}{\rho}\right) - \frac{1}{\rho}\left[\frac{\partial w}{\partial \boldsymbol{n}}\right] - \frac{1}{\rho c}\frac{\partial \rho}{\partial \boldsymbol{n}}\left[\frac{\partial w}{\partial t}\right]\right)\mathrm{d}\sigma_\xi \\ & + \frac{1}{4\pi(ct)^2}\int\int_{D\cap S(\boldsymbol{x},ct)}\left(w_0 - ct\frac{\partial w_0}{\partial \boldsymbol{n}} + tw_1\right)\mathrm{d}\sigma_\xi, \quad \boldsymbol{x} \in \partial D, \end{aligned} \tag{8}$$

where $\Theta(\boldsymbol{x})$ denotes the exterior solid angle at $\boldsymbol{x} \in \partial D$. For ∂D possessing a unique tangent plane at $\boldsymbol{x}$, $\Theta(\boldsymbol{x}) = 2\pi$, and as a result

$$\begin{aligned} w(\boldsymbol{x};t) = & -\frac{1}{2\pi}\int\int_{\partial D}\left([w]\frac{\partial}{\partial \boldsymbol{n}}\left(\frac{1}{\rho}\right) - \frac{1}{\rho}\left[\frac{\partial w}{\partial \boldsymbol{n}}\right] - \frac{1}{\rho c}\frac{\partial \rho}{\partial \boldsymbol{n}}\left[\frac{\partial w}{\partial t}\right]\right)\mathrm{d}\sigma_\xi \\ & + \frac{1}{2\pi(ct)^2}\int\int_{D\cap S(\boldsymbol{x},ct)}\left(w_0 - ct\frac{\partial w_0}{\partial \boldsymbol{n}} + tw_1\right)\mathrm{d}\sigma_\xi, \quad \boldsymbol{x} \in \partial D. \end{aligned} \tag{9}$$

Notice that the first integrals on the right-hand sides of (8) and (9) are *singular* integrals. The boundary integral equations (8) and (9) are not only the bases for us to derive the new NRBC, but also very useful

tools for solving initial-boundary value problems of wave equation in both bounded and unbounded domains. The derivation of the boundary integral equation (8) from (6) is very similar to that for Laplace's equation in three-dimension and its details are omitted here.

2.2. The new NRBC

First we introduce the original Kirchhoff-type exact NRBC proposed by Ting and Miksis [17]. The NRBC uses *two* artificial boundaries $\mathscr{B}$ and $\mathscr{S}$; the diagram is shown in Fig. 4. The computational domain is bounded by the surface of the scatterer γ and by the artificial boundary $\mathscr{B}$. The boundary $\mathscr{B}$ can be of any shape and the boundary $\mathscr{S}$, located inside the computation domain, contains all of the supports of $u_0(\cdot)$, $u_1(\cdot)$ and $f(\cdot,\tau)$ for $0 \leqslant \tau \leqslant T$. The exact NRBC of Ting–Miksis making use of the Kirchhoff formula (6) to the solution u of the wave equation (1) on the boundary $\mathscr{S}$ gives:

$$u(\boldsymbol{x};t) = -\frac{1}{4\pi}\int\int_{\mathscr{S}}\left([u]\frac{\partial}{\partial \boldsymbol{n}}\left(\frac{1}{\rho}\right) - \frac{1}{\rho}\left[\frac{\partial u}{\partial \boldsymbol{n}}\right] - \frac{1}{\rho c}\frac{\partial \rho}{\partial \boldsymbol{n}}\left[\frac{\partial u}{\partial t}\right]\right)\mathrm{d}\sigma_\xi, \quad \boldsymbol{x} \in \mathscr{B},$$

where u is the wave solution given by (1)–(4). This condition was not implemented numerically in [17]. Several years later, the FD implementation of this condition for the spherically symmetric case was carried out by Givoli and Cohen [8]. It was found that numerical scheme based on the Ting–Miksis condition exhibits numerically *instability* in long times. This instability may be eliminated by using a dissipative interior FD scheme as suggested by Givoli and Cohen.

The *new NRBC* is based on the boundary integral equation (8), which needs only one artificial boundary $\mathscr{S}$ of any shape; the set up is shown in Fig. 2. The computational domain Ω_i is bounded by the surface of the scatterer γ and by the artificial boundary $\mathscr{S}$. The boundary $\mathscr{S}$ is chosen to inclose all of the supports of $u_0(\cdot)$, $u_1(\cdot)$ and $f(\cdot,\tau)$ for $0 \leqslant \tau \leqslant T$. The new NRBC making use of the boundary integral Eq. (8) to the wave solution u on the artificial boundary $\mathscr{S}$ gives:

$$u(\boldsymbol{x};t)\left(1 - \frac{\Theta(\boldsymbol{x})}{4\pi}\right) = -\frac{1}{4\pi}\int\int_{\mathscr{S}}\left([u]\frac{\partial}{\partial \boldsymbol{n}}\left(\frac{1}{\rho}\right) - \frac{1}{\rho}\left[\frac{\partial u}{\partial \boldsymbol{n}}\right] - \frac{1}{\rho c}\frac{\partial \rho}{\partial \boldsymbol{n}}\left[\frac{\partial u}{\partial t}\right]\right)\mathrm{d}\sigma_\xi, \quad \boldsymbol{x} \in \mathscr{S}, \tag{10}$$

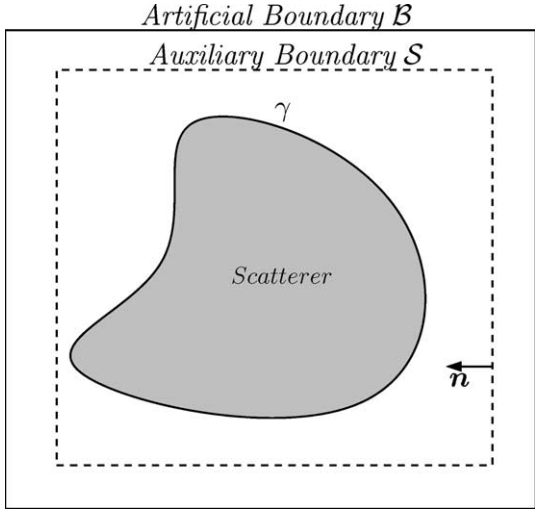

Fig. 4. Diagram for the Ting–Miksis NRBC.

where u is the wave solution given by (1)–(4) and the artificial boundary $\mathscr{S}$ is shown on Fig. 2. Notice that the right-hand side is a *singular* integral, where $\rho = |\boldsymbol{x} - \boldsymbol{\xi}|$, $\partial/\partial\boldsymbol{n}$ is the normal derivative at $\boldsymbol{\xi}$ on $\mathscr{S}$ and $\Theta(\boldsymbol{x})$ is the exterior solid angle at $\boldsymbol{x} \in \mathscr{S}$. The operator $[\cdot]$ is the retarded value operator, defined by (7). For a smooth artificial boundary $\mathscr{S}$, $\Theta(\boldsymbol{x}) = \pi/2$ and the new NRBC reduces to

$$u(\boldsymbol{x};t) = -\frac{1}{2\pi}\int\int_{\mathscr{S}}\left([u]\frac{\partial}{\partial\boldsymbol{n}}\left(\frac{1}{\rho}\right) - \frac{1}{\rho}\left[\frac{\partial u}{\partial\boldsymbol{n}}\right] - \frac{1}{\rho c}\frac{\partial\rho}{\partial\boldsymbol{n}}\left[\frac{\partial u}{\partial t}\right]\right)\mathrm{d}\sigma_\xi, \quad \boldsymbol{x} \in \mathscr{S}. \tag{11}$$

Since the boundary integral equation (10) or (11) involves both unknowns u and $\partial_{\boldsymbol{n}}u$ on the artificial boundary $\mathscr{S}$, the equation can not be solved independently and has to be solved in coupled with the interior wave equation, which may has variable coefficients or is nonlinear. Therefore the boundary integral equation can be considered as an exact artificial boundary condition for the interior wave equation.

The NRBC (10) or (11) is non-local in space and time. However, the temporal non-locality is restricted to a fixed amount of historical data, since the boundary integral (10) or (11) involves the retarded time $\tau = t - \rho/c$, which is bounded by

$$t - \rho_{\max}/c \leqslant \tau \leqslant t, \quad \text{where } \rho_{\max} = \max_{\boldsymbol{x},\boldsymbol{\xi}\in\mathscr{S}}|\boldsymbol{x} - \boldsymbol{\xi}|.$$

For example, if the artificial boundary $\mathscr{S}$ is a sphere with radius R, then $\rho_{\max} = 2R$ and the retarded time τ is in the interval $t - 2R/c \leqslant \tau \leqslant t$ and if the artificial boundary $\mathscr{S}$ is a cubic surface with side length L, then $\rho_{\max} = \sqrt{3}L$ and the retarded time τ is in the interval $t - \sqrt{3}L/c \leqslant \tau \leqslant t$. This means that the historical memory required by the NRBC does not grow in time and this is a main advantage of the present method.

3. One-dimensional spherically symmetric model

We consider the wave equation with spherically symmetric model, namely $f(\boldsymbol{x};t) = f(|\boldsymbol{x}|;t)$, $u_0(\boldsymbol{x}) = u_0(|\boldsymbol{x}|)$, $u_1(\boldsymbol{x}) = u_1(|\boldsymbol{x}|)$, and $\gamma = \{\boldsymbol{x}||\boldsymbol{x}| = r_\gamma\}$. Then the three-dimensional wave equation problem reduces to

$$\frac{\partial^2 v}{\partial t^2} - c^2\frac{\partial^2 v}{\partial r^2} = F(r;t) \quad \text{for } r \geqslant r_\gamma,\ t \geqslant 0 \tag{12}$$

$$v(r_\gamma;t) = r_\gamma g(t) \quad \text{for } t \geqslant 0 \tag{13}$$

$$v(r,0) = \partial_t v(r,0) = 0 \quad \text{for } r \geqslant r_\gamma, \tag{14}$$

where $r = |\boldsymbol{x}|$, $v(r;t) = ru(r;t)$ and $F(r;t) = rf(r;t)$. Here without loss of generality we assume $u_0 = u_1 = 0$.

We will show that for the one-dimensional symmetric model both continue and discrete version of the new NRBC are equivalent to that of the Engquist–Majda local NRBC [4].

3.1. Continuous version

For one-dimensional model with a spherical artificial boundary $\mathscr{S}$ of radius a (see the diagram of $\mathscr{S}$ in Fig. 5), the new NRBC (11) reduces to

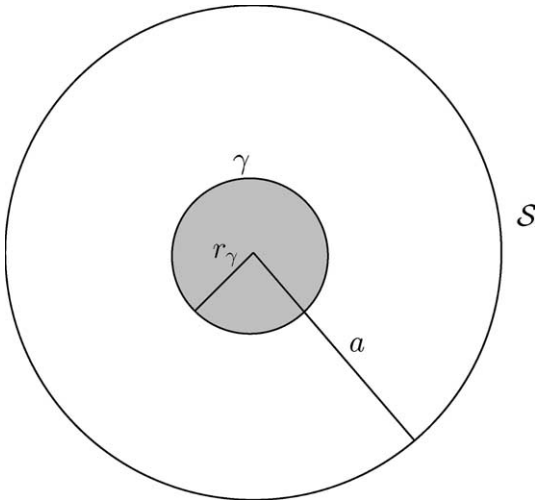

Fig. 5. Spherical artificial boundary $\mathscr{S}$.

$$\begin{aligned} u(a,t) = & -\frac{1}{2}\int_0^{\pi}\left\{u\left(a,t-\frac{2a}{c}\sin\left(\frac{\theta}{2}\right)\right)\right. \\ & \left.+2a\frac{\partial u}{\partial r}\left(a,t-\frac{2a}{c}\sin\left(\frac{\theta}{2}\right)\right)+\frac{2a}{c}\sin\left(\frac{\theta}{2}\right)\frac{\partial u}{\partial t}\left(a,t-\frac{2a}{c}\sin\left(\frac{\theta}{2}\right)\right)\right\}\cos\left(\frac{\theta}{2}\right)\mathrm{d}\theta \\ = & -\int_0^{2a/c}\left\{u(a,t-\alpha)+2a\frac{\partial u}{\partial r}(a,t-\alpha)+\alpha\frac{\partial u}{\partial t}(a,t-\alpha)\right\}\frac{c}{2a}\,\mathrm{d}\alpha. \end{aligned} \tag{15}$$

Using integration by parts for the third integrand gives

$$\int_0^{2a/c}\left\{\frac{\partial(ru)}{\partial t}(a,t-\alpha)+c\frac{\partial(ru)}{\partial r}(a,t-\alpha)\right\}\mathrm{d}\alpha=0.$$

Since the above equation holds for any t, on account of $u(r,t)$ and $\partial_t u(r,t)$ being zero for $t\leqslant 0$, we obtain

$$\frac{\partial(ru)}{\partial t}(a,t)+c\frac{\partial(ru)}{\partial r}(a,t)=0$$

or

$$\frac{\partial v}{\partial t}(a,t)+c\frac{\partial v}{\partial r}(a,t)=0.$$

This shows that for one-dimensional model the new NRBC is equivalent to the Engquist–Majda's local NRBC.

3.2. Discrete version

Assume that the numerical solution at the artificial boundary is denoted by $u^n(a)\approx u(a,t_n)$ with $t_n=n\Delta t$ and that the set $\{\alpha_m\,|\,m=0,\ldots,M\}$ is the grid points in the time interval $[0,2a/c]$ with $\alpha_0=0$ and

$\alpha_M = 2a/c$. Applying the trapezoidal rule to the first two integrands and the central-point rule to the third integrand of the NRBC (15) gives

$$\bar{\boldsymbol{u}}(a,t_n) = -\sum_{m=0}^{M} \Delta\alpha_m \{\bar{\boldsymbol{u}}(a,t_n-\alpha_m) + 2aD_r\bar{\boldsymbol{u}}(a,t_n-\alpha_m)\}\frac{c}{2a} - \sum_{m=1}^{M} \alpha_{m-1/2} D_t\bar{\boldsymbol{u}}(a,t_n-\alpha_{m-1/2})\Delta\alpha_{m-1/2}\frac{c}{2a}, \tag{16}$$

where $\alpha_m = 2a\sin(\theta_m/2)/c$ for $m = 0,1,\ldots,M$, $\theta_m = m\Delta\theta$ with $\Delta\theta = \pi/M$, $\alpha_{m-1/2} = (\alpha_m + \alpha_{m-1})/2$ and $\Delta\alpha_{m-1/2} = \alpha_m - \alpha_{m-1}$ for $m = 1,2,\ldots,M$, and

$$\Delta\alpha_m = \begin{cases} \alpha_{1/2} & \text{for } m = 0, \\ \alpha_{m+1/2} - \alpha_{m-1/2} & \text{for } m = 1,2,\ldots,M-1, \\ 2a/c - \alpha_{M-1/2} & \text{for } m = M. \end{cases}$$

Here $\bar{\boldsymbol{u}}(a,t)$ is an interpolation through

$$u^{l-1/2}(a) := \frac{u^l(a) + u^{l-1}(a)}{2} \quad \text{for } l = 1,\ldots,L,$$

where L has to satisfy $L\Delta t = 2a/c$. This interpolation has to satisfy the identity (17) given bellow. The difference quotients D_r and D_t are defined by

$$D_r\bar{\boldsymbol{u}}(a,\tau) = \frac{\bar{\boldsymbol{u}}(a,\tau) - \bar{\boldsymbol{u}}(a-h,\tau)}{h}$$

and

$$D_t\bar{\boldsymbol{u}}(a,t_n-\alpha_{m-1/2}) = \frac{\bar{\boldsymbol{u}}(a,t_n-\alpha_{m-1}) - \bar{\boldsymbol{u}}(a,t_n-\alpha_m)}{\alpha_m - \alpha_{m-1}}.$$

Some calculation on the above equation gives

$$\bar{\boldsymbol{u}}(a,t_n) - \bar{\boldsymbol{u}}(a,t_n-\alpha_M) = -\sum_{m=0}^{M} \Delta\alpha_m \{\bar{\boldsymbol{u}}(a,t_n-\alpha_m) + aD_r\bar{\boldsymbol{u}}(a,t_n-\alpha_m)\}\frac{c}{2a}$$

or

$$\begin{aligned} \sum_{l=1}^{L} D_t\bar{\boldsymbol{u}}(a,t_{n-l+1/2})\Delta t &= -\sum_{m=0}^{M} \Delta\alpha_m \{\bar{\boldsymbol{u}}(a,t_n-\alpha_m) + aD_r\bar{\boldsymbol{u}}(a,t_n-\alpha_m)\}\frac{c}{2a} \\ &= -\sum_{l=1}^{L} \Delta t\{u^{n-l+1/2}(a) + aD_r u^{n-l+1/2}(a)\}\frac{c}{2a}. \end{aligned} \tag{17}$$

We notice that the last identity in (17) is satisfied by an *integral-average* interpolation for $\bar{\boldsymbol{u}}(a,t_n-\alpha_m)$ defined by

$$\bar{\boldsymbol{u}}(a,t_n-\alpha_m) := \frac{1}{\Delta\alpha_m}\int_{t_n-\alpha_{m+1/2}}^{t_n-\alpha_{m-1/2}} \bar{\boldsymbol{u}}_{\Delta t}(a,\tau)\,\mathrm{d}\tau$$

under the condition $\Delta\alpha_m < \Delta t$ for all $m = 0,1,\ldots,M$, where $\bar{\boldsymbol{u}}_{\Delta t}(a,\tau)$ is a piecewise constant function defined by $\bar{\boldsymbol{u}}_{\Delta t}(a,\tau) := u^{l+1/2}(a)$ for $\tau \in [t_l, t_{l+1}]$, $\alpha_{-1/2} = 0$ and $\alpha_{M+1/2} = 2a/c$. An *integral-average* interpolation for $D_r\bar{\boldsymbol{u}}(a,t_n-\alpha_m)$ can be defined similarly.

We have to point out that a sufficient condition for $\Delta\alpha_m < \Delta t$ is that

$$\Delta\theta = \pi/M < \Delta t. \tag{18}$$

This gives an important relationship between the boundary integral step $\Delta\theta$ and the interior time step Δt.

Since the above equation holds for all n, on account of $\bar{u}(a,\tau)$ being zero for $\tau < 0$, we can deduce that

$$D_t(r\bar{u})(a,t_{n-1/2}) + c(\bar{u}(a,t_{n-1/2}) + aD_r\bar{u}(a,t_{n-1/2})) = 0$$

or

$$D_t(r\bar{u})(a,t_{n-1/2}) + cD_r(r\bar{u})(a,t_{n-1/2}) = 0. \tag{19}$$

This is a discrete version of

$$\frac{\partial v}{\partial t}(a,t) + c\frac{\partial v}{\partial r}(a,t) = 0.$$

Therefore, we have shown that both the continue version (15) and the discrete version (16) of the new NRBC are equivalent to that of the local Engquist–Majda NRBC.

3.3. Numerical test and long-time stability

In this section, we will repeat the numerical test given by Givoli and Cohen in [8] by using our new NRBC. The main objective of this subsection is to test the long-time stability of the proposed method.

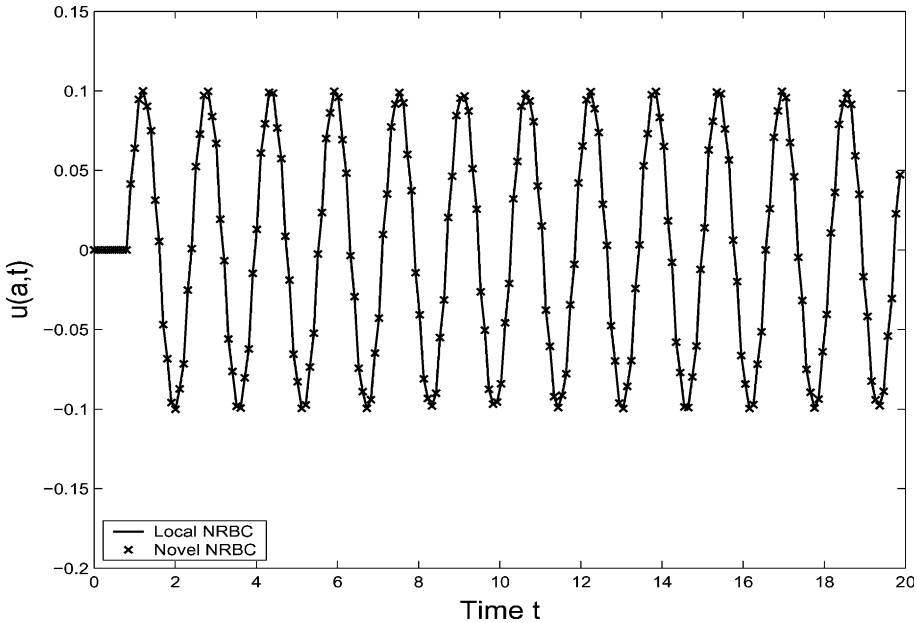

Fig. 6. The numerical solutions $u(a,t)$ obtained by using the local NRBC (19) and the new NRBC (16), for $g(t) = \sin 4t$ and the parameters $a = 1$, $h = 0.9/180 = 0.005$, $\Delta t = 0.003656$ and $\Delta\theta = \pi/1000 = 0.0031415926$.

For the test problem, $f \equiv 0$ or $F \equiv 0$ in (12) and the exact solution of (12)–(14) is given by

$$v(r,t) = \begin{cases} 0, & t < (r - r_\gamma)/c, \\ r_\gamma g(t - (r - r_\gamma))/c, & t \geqslant (r - r_\gamma)/c. \end{cases} \tag{20}$$

The one-dimensional wave equation (12) in the computational domain $r_\gamma \leqslant r \leqslant a$ is solved by the standard non-dissipative central difference scheme

$$u_j^{n+1} = 2u_j^n - u_j^{n-1} + \left(\frac{c\Delta t}{h}\right)(u_{j+1}^n - 2u_j^n + u_{j-1}^n),$$

where $h = (a - r_\gamma)/K$ is the mesh size in space with K a given positive integer, and Δt is a time step satisfying the stability condition $c\Delta t/h \leqslant 1$.

At the artificial boundary $r = a$ two discrete artificial boundary conditions are used for the purpose of comparison: the new NRBC (16) and the local Engquist–Majda NRBC (19).

In numerical computation we set $c = 1$, $r_\gamma = 0.1$ and $a = 1$ and take $g(t) = \sin \omega t$. The parameters we choose are that the space step $h = 0.9/180 = 0.005$, the time step $\Delta t = 0.003656 < h$ satisfying the stability condition, the boundary integral step $\Delta\theta = \pi/1000 = 0.0031415926 < \Delta t$ satisfying the relationship condition (18), and the frequency $\omega = 4$. Fig. 6 shows the two numerical solutions at $r = a = 1$ as a function of time. From Fig. 6 we see that the new NRBC solution coincides with the local NRBC solution, which verifies the theoretical result given in the above subsection: the discrete version of the new NRBC (16) is equivalent to that of the local Engquist–Majda NRBC (19). Both numerical solutions agree with the exact solution very well for all time $0 \leqslant t \leqslant 20$ and the solution by using the new NRBC never develops instability. In contrast, the solution obtained by using the Ting–Miksis NRBC starts to develop a clear instability at about $t = 7$ (see [8]).

4. Cubic artificial boundary

In this section, we apply the NRBC (10) to a cubic artificial boundary (see Fig. 7) and give details description of the NRBC on the cubic boundary.

The cubic artificial boundary of side length $2a$ is plotted in Fig. 7, which consists of six *faces*:

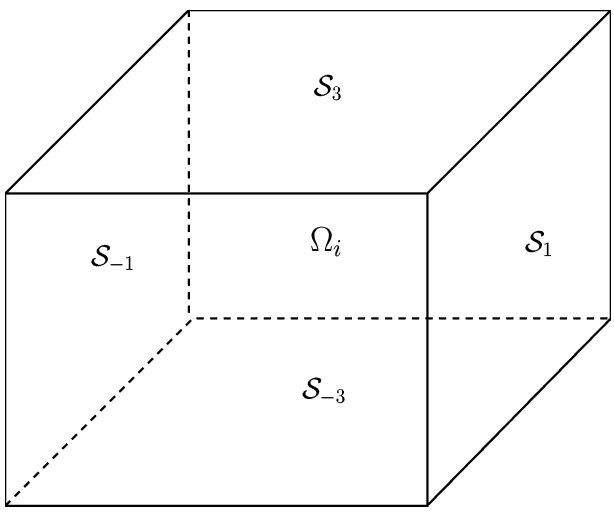

Fig. 7. Cubic artificial boundary: $\mathscr{S} = \cup_{l \in \mathscr{L}} \mathscr{S}_l$.

$$\mathscr{S}_l = \{(\xi_1, \xi_2, \xi_3) | \xi_{|l|} = \mathrm{sign}(l)a, -a < \xi_j < a, j \neq |l|\}$$

for each $l \in \mathscr{L}$, where

$$\mathscr{L} := \{-3, -2, -1, 1, 2, 3\}.$$

We use the notation $\mathscr{E}_{l,s}$ for $l, s \in \mathscr{L}$ and $|l| \neq |s|$ to denote 12 *edges* of the cube:

$$\mathscr{E}_{l,s} := \{(\xi_1, \xi_2, \xi_3) | \xi_{|l|} = \mathrm{sign}(l)a, \xi_{|s|} = \mathrm{sign}(s)a, -a < \xi_j < a, j \neq |l|, |s|\},$$

and the notation $\mathscr{C}_{l,s,m}$ for $l, s, m \in \mathscr{L}$ and $|l| \neq |s| \neq |m|$ to denote eight *vertices* of the cube:

$$\mathscr{C}_{l,s,m} := \{(\xi_1, \xi_2, \xi_3) | \xi_{|l|} = \mathrm{sign}(l)a, \xi_{|s|} = \mathrm{sign}(s)a, \xi_{|m|} = \mathrm{sign}(m)a\}.$$

We have to point out that $\Theta(\boldsymbol{x})$ given in (10) assumes difference value for $\boldsymbol{x}$ being a face point, an edge point or a vortex point. More precisely, $\Theta(\boldsymbol{x}) = \pi/2$ for $\boldsymbol{x} \in \mathscr{S}_l$, $\Theta(\boldsymbol{x}) = \pi/4$ for $\boldsymbol{x} \in \mathscr{E}_{l,s}$ and $\Theta(\boldsymbol{x}) = \pi/8$ for $\boldsymbol{x} \in \mathscr{C}_{l,s,m}$. The new NRBC (10) applied to cubic surface gives the following three kinds of expressions.

(1) Let $\boldsymbol{x} \in \mathscr{S}_l$. More precisely, assume $\boldsymbol{x} = (a, x_2, x_3) \in \mathscr{S}_1$, then we have

$$\begin{aligned} u(a, x_2, x_3, t) = & -\frac{1}{2\pi} \int\int_{\mathscr{S}_1} \frac{1}{\rho} \left[\frac{\partial u}{\partial x_1}\right] \mathrm{d}\sigma_1 - \frac{1}{2\pi} \sum_{\substack{l \in \mathscr{L} \\ l \neq 1}} \int\int_{\mathscr{S}_l} \frac{\mathrm{sign}(l)}{\rho} \\ & \times \left\{ \left([u] \frac{1}{\rho} + \left[\frac{\partial u}{\partial t}\right] \frac{1}{c} \right) \frac{\xi_{|l|} - x_{|l|}}{\rho} + \left[\frac{\partial u}{\partial x_{|l|}}\right] \right\} \mathrm{d}\sigma_l, \end{aligned} \tag{21}$$

where $\mathrm{d}\sigma_l = \mathrm{d}\xi_i \mathrm{d}\xi_j$ with $i \neq |l|$, $j \neq |l|$ and $i \neq j$. For other cases we have formulas similar to (21).

(2) Let $\boldsymbol{x} \in \mathscr{E}_{l,s}$. More precisely, assume $\boldsymbol{x} = (a, a, x_3) \in \mathscr{E}_{1,2}$, then we have

$$\begin{aligned} u(a, a, x_3, t) = & -\frac{1}{3\pi} \left\{ \int\int_{\mathscr{S}_1} \frac{1}{\rho} \left[\frac{\partial u}{\partial x_1}\right] \mathrm{d}\sigma_1 + \int\int_{\mathscr{S}_2} \frac{1}{\rho} \left[\frac{\partial u}{\partial x_2}\right] \mathrm{d}\sigma_2 \right\} - \frac{1}{3\pi} \sum_{\substack{l \in \mathscr{L} \\ l \neq 1,2}} \int\int_{\mathscr{S}_l} \frac{\mathrm{sign}(l)}{\rho} \\ & \times \left\{ \left([u] \frac{1}{\rho} + \left[\frac{\partial u}{\partial t}\right] \frac{1}{c} \right) \frac{\xi_{|l|} - x_{|l|}}{\rho} + \left[\frac{\partial u}{\partial x_{|l|}}\right] \right\} \mathrm{d}\sigma_l. \end{aligned} \tag{22}$$

Results for other edges can obtained in a similar way.

(3) Let $\boldsymbol{x} \in \mathscr{C}_{l,s,m}$. More precisely, assume $\boldsymbol{x} = (a, a, a) \in \mathscr{E}_{1,2,3}$, then we have

$$\begin{aligned} u(a, a, a, t) = & -\frac{2}{7\pi} \left\{ \int\int_{\mathscr{S}_1} \frac{1}{\rho} \left[\frac{\partial u}{\partial x_1}\right] \mathrm{d}\sigma_1 + \int\int_{\mathscr{S}_2} \frac{1}{\rho} \left[\frac{\partial u}{\partial x_2}\right] \mathrm{d}\sigma_2 + \int\int_{\mathscr{S}_3} \frac{1}{\rho} \left[\frac{\partial u}{\partial x_1}\right] \mathrm{d}\sigma_3 \right\} \\ & - \frac{2}{7\pi} \sum_{\substack{l \in \mathscr{L} \\ l \neq 1,2,3}} \int\int_{\mathscr{S}_l} \frac{\mathrm{sign}(l)}{\rho} \left\{ \left([u] \frac{1}{\rho} + \left[\frac{\partial u}{\partial t}\right] \frac{1}{c} \right) \frac{\xi_{|l|} - x_{|l|}}{\rho} + \left[\frac{\partial u}{\partial x_{|l|}}\right] \right\} \mathrm{d}\sigma_l. \end{aligned} \tag{23}$$

Formulas for other vertices can be derived similarly.

5. Numerical scheme

In this section, we will use a FD method to solve (1)–(4) in the computational domain Ω_i, incorporating a numerical approximation to the new NRBC (21)–(23) on cubic artificial boundary to provide appropriate data on the artificial boundary.

5.1. Non-dissipative central difference scheme in Ω_i

We choose a standard explicit central difference scheme. The wave equation (1) is discretized both in time and in space at $(\boldsymbol{x};t)=(x_1,x_2,x_3;t)$ using second-order central differences. We denote by $u_{\boldsymbol{i}}^n$ the numerical grid function at $(\boldsymbol{x}_{\boldsymbol{i}};t_n)=(i_1h,i_2h,i_3h;n\Delta t)$, where $\boldsymbol{i}=(i_1,i_2,i_3)\in\mathbb{Z}^3$, $h=a/K$ with some given $K\in\mathbb{N}$ is the mesh size in space step uniform in the x_1, x_2 and x_3 directions, and Δt is the time step. The stability condition $c\Delta t/h\leqslant 1/\sqrt{3}$ is satisfied. The central difference scheme is given in the following form

$$u_{\boldsymbol{i}}^{n+1}=2u_{\boldsymbol{i}}^n-u_{\boldsymbol{i}}^{n-1}+\left(\frac{c\Delta t}{h}\right)^2\left(u^n_{i_1-1,i_2,i_3}+u^n_{i_1+1,i_2,i_3}+u^n_{i_1,i_2-1,i_3}+u^n_{i_1,i_2+1,i_3}+u^n_{i_1,i_2,i_3-1}+u^n_{i_1,i_2,i_3+1}-6u^n_{i_1,i_2,i_3}\right)+f(\boldsymbol{x}_{\boldsymbol{i}},t_n)(\Delta t)^2. \tag{24}$$

5.2. Numerical approximation to the NRBC (21)–(23)

One of the advantages of using cubic artificial boundary is that we can apply only one set of mesh grid to both inside of and on boundary of the cube. There are three kinds of boundary mesh: *face mesh* $\sigma_{\boldsymbol{j}}^{\mathscr{S}_l}$ with center at $\boldsymbol{x}_{\boldsymbol{j}}=(j_1h,j_2h,j_3h)\in\mathscr{S}_l$, *edge mesh* $\sigma_{\boldsymbol{j}}^{\mathscr{E}_{l,m}}$ with center at $\boldsymbol{x}_{\boldsymbol{j}}\in\mathscr{E}_{l,m}$ and *vertex mesh* $\sigma_{\boldsymbol{j}}^{\mathscr{C}_{l,m,s}}$ with center at $\boldsymbol{x}_{\boldsymbol{j}}\in\mathscr{C}_{l,m,s}$ indicated in Fig. 8, where the three kinds of meshes are defined by

$$\sigma_{\boldsymbol{j}}^{\mathscr{S}_l}:=\{(\xi_1,\xi_2,\xi_3)|\xi_{|l|}=\operatorname{sign}(l)a,|\xi_m-j_mh|<h/2,|\xi_s-j_sh|<h/2;\ \ m,s\neq|l|\},$$

$$\begin{aligned}\sigma_{\boldsymbol{j}}^{\mathscr{E}_{l,m}}:=&\{(\xi_1,\xi_2,\xi_3)|\xi_{|l|}=\operatorname{sign}(l)a,0<(a-\operatorname{sign}(m)\xi_{|m|})<h/2,|\xi_s-j_sh|<h/2,\quad s\neq|l|,|m|\}\\&\cup\{(\xi_1,\xi_2,\xi_3)|\xi_{|m|}=\operatorname{sign}(m)a,0<(a-\operatorname{sign}(l)\xi_{|l|})<h/2,|\xi_s-j_sh|<h/2,\quad s\neq|l|,|m|\}\end{aligned}$$

and

$$\begin{aligned}\sigma_{\boldsymbol{j}}^{\mathscr{C}_{l,m,s}}:=&\{(\xi_1,\xi_2,\xi_3)|\xi_{|l|}=\operatorname{sign}(l)a,0<(a-\operatorname{sign}(m)\xi_{|m|})<h/2,0<(a-\operatorname{sign}(s)\xi_{|s|})<h/2\}\\&\cup\{(\xi_1,\xi_2,\xi_3)|\xi_{|m|}=\operatorname{sign}(m)a,0<(a-\operatorname{sign}(l)\xi_{|l|})<h/2,0<(a-\operatorname{sign}(s)\xi_{|s|})<h/2\}\\&\cup\{(\xi_1,\xi_2,\xi_3)|\xi_{|s|}=\operatorname{sign}(s)a,0<(a-\operatorname{sign}(m)\xi_{|m|})<h/2,0<(a-\operatorname{sign}(l)\xi_{|l|})<h/2\}.\end{aligned}$$

It is easy to see from Fig. 8 that

$$|\sigma_{\boldsymbol{j}}^{\mathscr{S}_l}|=|\sigma_{\boldsymbol{j}}^{\mathscr{E}_{l,m}}|=h^2,|\sigma_{\boldsymbol{j}}^{\mathscr{C}_{l,m,s}}|=3h^2/4,$$

where $|\sigma|$ denotes the measure of σ.

Let $\boldsymbol{x}$ and t at the left-hand sides of the NRBC (21)–(23) be evaluated at boundary grid mesh point $\boldsymbol{x}=\boldsymbol{x}_{\boldsymbol{i}}$ and time mesh point $t=t_n$ respectively. Then (21)–(23) can be written as a sum of the following integrals on face mesh, edge mesh and vertex mesh:

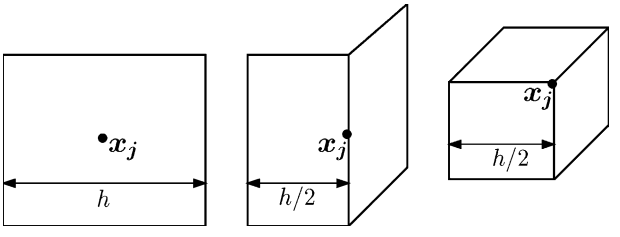

Fig. 8. From left to right are face mesh $\sigma_{\boldsymbol{j}}^{\mathscr{S}_l}$, edge mesh $\sigma_{\boldsymbol{j}}^{\mathscr{E}_{l,m}}$ and vertex mesh $\sigma_{\boldsymbol{j}}^{\mathscr{C}_{l,m,s}}$ with their center at $\boldsymbol{x}_{\boldsymbol{j}}$.

$$\mathrm{I} = \int\int_{\sigma_j^{\mathscr{S}_l}} \frac{1}{|\boldsymbol{x_i}-\boldsymbol{\xi}|^p} F(\boldsymbol{\xi}; t_n - |\boldsymbol{x_i}-\boldsymbol{\xi}|/c)\,\mathrm{d}\sigma_\xi,$$

$$\mathrm{II} = \int\int_{\sigma_j^{\mathscr{E}_{l,m}}} \frac{1}{|\boldsymbol{x_i}-\boldsymbol{\xi}|^p} F(\boldsymbol{\xi}; t_n - |\boldsymbol{x_i}-\boldsymbol{\xi}|/c)\,\mathrm{d}\sigma_\xi$$

and

$$\mathrm{III} = \int\int_{\sigma_j^{\mathscr{C}_{l,m,s}}} \frac{1}{|\boldsymbol{x_i}-\boldsymbol{\xi}|^p} F(\boldsymbol{\xi}; t_n - |\boldsymbol{x_i}-\boldsymbol{\xi}|/c)\,\mathrm{d}\sigma_\xi,$$

where $p = 1, 2$ and $F(\boldsymbol{\xi};\tau) = u(\boldsymbol{\xi};\tau), \partial_{\boldsymbol{n}} u(\boldsymbol{\xi};\tau)$ or $\partial_t u(\boldsymbol{\xi};\tau)$ and $\sigma_j^{\mathscr{S}_l}$, $\sigma_j^{\mathscr{E}_{l,m}}$ and $\sigma_j^{\mathscr{C}_{l,m,s}}$ stand for face mesh, edge mesh and vertex mesh on the cubic boundary respectively. Therefore, we can give an approximation to the NRBC (21)–(23) through approximations to I, II and III.

For $\sigma_i^{\mathscr{S}_l}$, $\sigma_i^{\mathscr{E}_{l,m}}$ and $\sigma_i^{\mathscr{C}_{l,m,s}}$ with center at the evaluating mesh point $\boldsymbol{x_i}$, we use the following approximations to I, II and III for $p = 1$:

$$\begin{aligned}\int\int_{\sigma_i^{\mathscr{S}_l}} \frac{1}{|\boldsymbol{x_i}-\boldsymbol{\xi}|} F(\boldsymbol{\xi}; t_n - |\boldsymbol{x_i}-\boldsymbol{\xi}|/c)\,\mathrm{d}\sigma_\xi &\approx F(\boldsymbol{x_i}; t_n)\int\int_{\sigma_i^{\mathscr{S}_l}} \frac{1}{|\boldsymbol{x_i}-\boldsymbol{\xi}|}\,\mathrm{d}\sigma_\xi \\ &= 4h\log(1+\sqrt{2})F(\boldsymbol{x_i}; t_n),\end{aligned} \tag{25}$$

$$\begin{aligned}\int\int_{\sigma_i^{\mathscr{E}_{l,m}}} \frac{1}{|\boldsymbol{x_i}-\boldsymbol{\xi}|} F(\boldsymbol{\xi}; t_n - |\boldsymbol{x_i}-\boldsymbol{\xi}|/c)\,\mathrm{d}\sigma_\xi &\approx F(\boldsymbol{x_i}; t_n)\int\int_{\sigma_i^{\mathscr{E}_{l,m}}} \frac{1}{|\boldsymbol{x_i}-\boldsymbol{\xi}|}\,\mathrm{d}\sigma_\xi \\ &= 4h\log(1+\sqrt{2})F(\boldsymbol{x_i}; t_n),\end{aligned} \tag{26}$$

$$\begin{aligned}\int\int_{\sigma_i^{\mathscr{C}_{l,m,s}}} \frac{1}{|\boldsymbol{x_i}-\boldsymbol{\xi}|} F(\boldsymbol{\xi}; t_n - |\boldsymbol{x_i}-\boldsymbol{\xi}|/c)\,\mathrm{d}\sigma_\xi &\approx F(\boldsymbol{x_i}; t_n)\int\int_{\sigma_i^{\mathscr{C}_{l,m,s}}} \frac{1}{|\boldsymbol{x_i}-\boldsymbol{\xi}|}\,\mathrm{d}\sigma_\xi \\ &= 3h\log(1+\sqrt{2})F(\boldsymbol{x_i}; t_n).\end{aligned} \tag{27}$$

We have to notice that since $\boldsymbol{x_i}$ is the center of the domains of the integrals, the integrands including a factor $1/|\boldsymbol{x_i}-\boldsymbol{\xi}|$ are singular. Therefore, in the above approximations only well-behaved function F of the variable $\boldsymbol{\xi}$ is assumed at $\boldsymbol{x_i}$, where the retarded time-histories are zero. In this case, integrating the singular integrands results in (25)–(27).

For $\sigma_j^{\mathscr{S}_l}$, $\sigma_j^{\mathscr{E}_{l,m}}$ and $\sigma_j^{\mathscr{C}_{l,m,s}}$ with center at $\boldsymbol{x_j} \neq \boldsymbol{x_i}$, using the central-point rule to I, II and III gives:

$$\int\int_{\sigma_j^{\mathscr{S}_l}} \frac{1}{|\boldsymbol{x_i}-\boldsymbol{\xi}|^p} F(\boldsymbol{\xi}; t_n - |\boldsymbol{x_i}-\boldsymbol{\xi}|/c)\,\mathrm{d}\sigma_\xi \approx \frac{h^2}{|\boldsymbol{x_i}-\boldsymbol{x_j}|^p} F(\boldsymbol{x_j}; t_n - |\boldsymbol{x_i}-\boldsymbol{x_j}|/c), \tag{28}$$

$$\int\int_{\sigma_j^{\mathscr{E}_{l,m}}} \frac{1}{|\boldsymbol{x_i}-\boldsymbol{\xi}|^p} F(\boldsymbol{\xi}; t_n - |\boldsymbol{x_i}-\boldsymbol{\xi}|/c)\,\mathrm{d}\sigma_\xi \approx \frac{h^2}{|\boldsymbol{x_i}-\boldsymbol{x_j}|^p} F(\boldsymbol{x_j}; t_n - |\boldsymbol{x_i}-\boldsymbol{x_j}|/c), \tag{29}$$

$$\int\int_{\sigma_j^{\mathscr{C}_{l,m,s}}} \frac{1}{|\boldsymbol{x_i}-\boldsymbol{\xi}|^p} F(\boldsymbol{\xi}; t_n - |\boldsymbol{x_i}-\boldsymbol{\xi}|/c)\,\mathrm{d}\sigma_\xi \approx \frac{3h^2/4}{|\boldsymbol{x_i}-\boldsymbol{x_j}|^p} F(\boldsymbol{x_j}; t_n - |\boldsymbol{x_i}-\boldsymbol{x_j}|/c). \tag{30}$$

Using the above approximations gives an approximation to the integrals in (21)–(23). In general, the approximation is only a first order approximation, but the numerical formulae are simple and easy to program. Therefore we use the scheme to test stability, accuracy and convergence of the new NRBC. High-order approximation can be obtained by using more accurate numerical integrations.

What we need next is to provide a numerical approximation to $\partial_{\boldsymbol{n}} u(\boldsymbol{\xi};\tau)$ and $\partial_t u(\boldsymbol{\xi};\tau)$ on the cubic boundary and a time interpolation approximation to $F(\boldsymbol{\xi};\tau)$ for $\tau \in [t_n, t_{n+1}]$. This will be outlined below:

(1) Linear interpolation for $F(\boldsymbol{\xi};\tau)$. For $\tau \in [t_n, t_{n+1}]$, we define

$$F(\boldsymbol{\xi};\tau) := F(\boldsymbol{\xi};t_n)\frac{t_{n+1}-\tau}{\Delta t} + F(\boldsymbol{\xi};t_{n+1})\frac{\tau - t_n}{\Delta t}.$$

(2) Numerical time derivatives

$$\frac{\partial u(\boldsymbol{\xi},\tau)}{\partial t} \approx \frac{u(\boldsymbol{\xi},\tau+\Delta t) - u(\boldsymbol{\xi},\tau-\Delta t)}{2\Delta t}.$$

(3) Numerical normal derivatives to $\mathscr{S}$. Here we only need to consider numerical approximation to $\partial_{\boldsymbol{n}} u(\boldsymbol{x_j};\tau)$, where $\boldsymbol{x_j}$ is a boundary mesh point.

(a) If $\boldsymbol{x_j}$ is a center of a face mesh, for instance, $\sigma_j^{\mathscr{S}_1}$, then

$$\partial_{\boldsymbol{n}} u(\boldsymbol{x_j};\tau) = -\partial_{x_1} u(\boldsymbol{x_j};\tau),$$

which is approximated by using one side difference quotient

$$\partial_{\boldsymbol{n}} u(\boldsymbol{x_j};\tau) \approx \frac{u(\boldsymbol{x_j};\tau) - u(\boldsymbol{x_j}-\boldsymbol{h}_1;\tau)}{h},$$

where $\boldsymbol{h}_1 = (h,0,0)$.

(b) If $\boldsymbol{x_j}$ is a center of a edge mesh, for instance, $\sigma_j^{\mathscr{E}_{1,2}}$, then

$$\partial_{\boldsymbol{n}} u(\boldsymbol{x_j};\tau) = -\frac{1}{2}\left(\partial_{x_1} u(\boldsymbol{x_j};\tau) + \partial_{x_2} u(\boldsymbol{x_j};\tau)\right) = \frac{1}{\sqrt{2}}\partial_{\boldsymbol{\gamma}} u(\boldsymbol{x_j};\tau),$$

where $\boldsymbol{\gamma}$ is the diagonal direction joining $\boldsymbol{x_j}$ to $\boldsymbol{x_j}-\boldsymbol{h}_1-\boldsymbol{h}_2$ with $\boldsymbol{h}_2 = (0,h,0)$. Using one side difference quotient to approximate the last directional derivative gives

$$\partial_{\boldsymbol{n}} u(\boldsymbol{x_j};\tau) \approx \frac{1}{\sqrt{2}}\frac{u(\boldsymbol{x_j};\tau) - u(\boldsymbol{x_j}-\boldsymbol{h}_1-\boldsymbol{h}_2;\tau)}{\sqrt{2}h} = \frac{u(\boldsymbol{x_j};\tau) - u(\boldsymbol{x_j}-\boldsymbol{h}_1-\boldsymbol{h}_2;\tau)}{2h}.$$

(c) If $\boldsymbol{x_j}$ is a center of a vertex mesh, for instance, $\sigma_j^{\mathscr{C}_{1,2,3}}$, then

$$\partial_{\boldsymbol{n}} u(\boldsymbol{x_j};\tau) = -\frac{1}{3}\left(\partial_{x_1} u(\boldsymbol{x_j};\tau) + \partial_{x_2} u(\boldsymbol{x_j};\tau) + \partial_{x_3} u(\boldsymbol{x_j};\tau)\right) = \frac{1}{\sqrt{3}}\partial_{\boldsymbol{\gamma}} u(\boldsymbol{x_j};\tau),$$

where $\boldsymbol{\gamma}$ is the diagonal direction joining $\boldsymbol{x_j}$ to $\boldsymbol{x_j}-\boldsymbol{h}_1-\boldsymbol{h}_2-\boldsymbol{h}_3$ with $\boldsymbol{h}_3 = (0,0,h)$. Using one side difference quotient to approximate the last directional derivative gives

$$\partial_{\boldsymbol{n}} u(\boldsymbol{x_j};\tau) \approx \frac{1}{\sqrt{3}}\frac{u(\boldsymbol{x_j};\tau) - u(\boldsymbol{x_j}-\boldsymbol{h}_1-\boldsymbol{h}_2-\boldsymbol{h}_3;\tau)}{\sqrt{3}h} = \frac{u(\boldsymbol{x_j};\tau) - u(\boldsymbol{x_j}-\boldsymbol{h}_1-\boldsymbol{h}_2-\boldsymbol{h}_3;\tau)}{3h}.$$

With the above description of the numerical scheme in the interior of Ω_i and the numerical approximation to the proposed NRBC on its boundary, we can proceed to compute the numerical solution as follows:

(1) Initialize the starting values u_j^0 and u_j^{-1} from $u_0(\boldsymbol{x})$ and $u_1(\boldsymbol{x})$ given in (3) and (4), respectively.

(2) Compute u_j^{n+1} at all interior grid points in the cubic computational domain using (24).

(3) Compute u_j^{n+1} at all grid points on the cubic surface using the discretizations (21)–(23).
(4) Repeat the procedure (2) and (3) for $n = 0, 1, \ldots$ and get the whole numerical solution u_j^n for $n = 1, 2, \ldots$

6. Three-dimensional numerical experiments

In order to test the accuracy and stability of the proposed boundary condition, we consider an initial value problem in $\boldsymbol{R}^3$ with zero initial conditions:

$$\begin{aligned}
&\frac{\partial^2 u}{\partial t^2} = \nabla^2 u + f(\boldsymbol{x}, t) \quad \text{in } \boldsymbol{R}^3 \times (0, T),\\
&u(\boldsymbol{x}, 0) = 0 \quad \text{in } \boldsymbol{R}^3,\\
&\partial_t u(\boldsymbol{x}, 0) = 0 \quad \text{in } \boldsymbol{R}^3,
\end{aligned}$$

where

$$f(\boldsymbol{x}, t) = f(|\boldsymbol{x}|, t) = \begin{cases} \sin(\omega t)(1 - |\boldsymbol{x}|^2/a^2)^2 & |\boldsymbol{x}| < a,\\ 0 & |\boldsymbol{x}| \geqslant a. \end{cases} \tag{31}$$

It is easy to show that the exact solution is spherically symmetric, i.e., $u(\boldsymbol{x}; t) = u(|\boldsymbol{x}|; t)$ and $v(r; t) = ru(r; t)$ satisfies the one-dimensional wave equation (12) with zero initial data. Thus $u(|\boldsymbol{x}|, t)$ has an explicit expression through one-dimensional wave equation

$$\begin{aligned}
u(|\boldsymbol{x}|, t) &= \frac{1}{2|\boldsymbol{x}|} \int_0^t \int_{|\boldsymbol{x}|-(t-\tau)}^{|\boldsymbol{x}|+(t-\tau)} r f(|r|, \tau)\, \mathrm{d}r\, \mathrm{d}\tau\\
&= -\frac{1}{12|\boldsymbol{x}|} \int_{\min[|\boldsymbol{x}|,1]}^{\min[|\boldsymbol{x}|+t,1]} \sin[\omega(t - r + |\boldsymbol{x}|)](1 - r^2)^3\, \mathrm{d}r\\
&\quad + \frac{1}{12|\boldsymbol{x}|} \int_{\min[\max[|\boldsymbol{x}|-t,-1],1]}^{\min[|\boldsymbol{x}|,1]} \sin[\omega(t + r - |\boldsymbol{x}|)](1 - r^2)^3\, \mathrm{d}r.
\end{aligned}$$

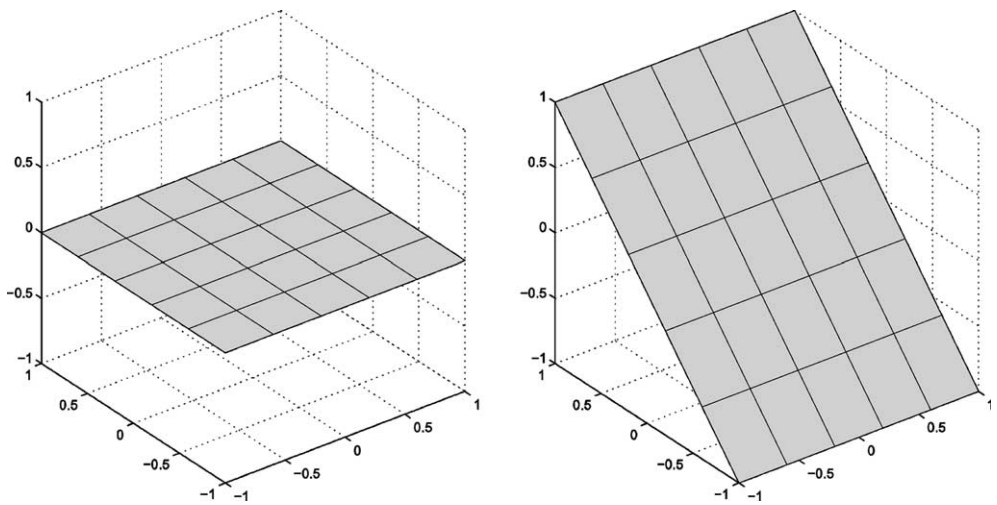

Fig. 9. Two sample slice planes from the computational domain Ω_i.

The close form solution $u(|\boldsymbol{x}|,t)$ can be obtained by using MATHEMATICA software to carry out the last two integrals and a C or Fortran language programm for evaluation of $u(|\boldsymbol{x}|,t)$ can be easily obtained by using the software's CForm or FortranForm function. Since the close form solution and its evaluation programm are quite long, we omit the details here. Therefore, we can estimate the accuracy and convergence rate numerically for the numerical scheme using the discretization for the new NRBC. Notice that even though the solution is spherically symmetric, the artificial boundary (cubic surface) is not spherically symmetric. Thus the numerical computation is a full three-dimension one.

In numerical tests we choose computational domain Ω_i being a cube with side length $2a = 2$, mesh size $h = 10^{-1}, 20^{-1}, 30^{-1}, 40^{-1}, 80^{-1}$ being same in all three directions, time step $\Delta t = h/2$ satisfying the stability condition $\Delta t/h \leqslant 1/\sqrt{3}$, and frequency $\omega = 2, 3$ and 4. Notice that here the artificial cubic surface with side length $2a = 2$ just contains the space support of $f(\boldsymbol{x},t)$ defined by (31). In order to show the numerical results we choose two sample slice planes from the cubic computational domain, indicated in Fig 9. We use $u_h(\boldsymbol{x};t)$ to denote the numerical solution with space step size h.

In Figs. 10–13 the numerical solution and the exact solution are shown on left-hand side and right-hand side respectively, where their date come from the left slice plane or right slice plane of Fig. 9.

We consider the L^2-error defined by

$$\|u(\cdot;t) - u_h(\cdot;t)\|_{L^2(\Omega_i)}$$

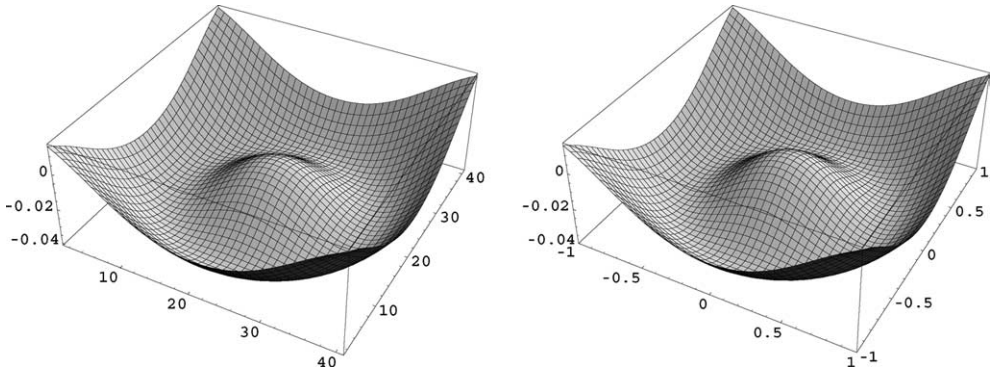

Fig. 10. The right-hand figure is exact solution and the left-hand is numerical solution at time $t = 4$ with $\omega = 2$ and $h = 2/40$, their date come from the left slice plane of Fig. 9.

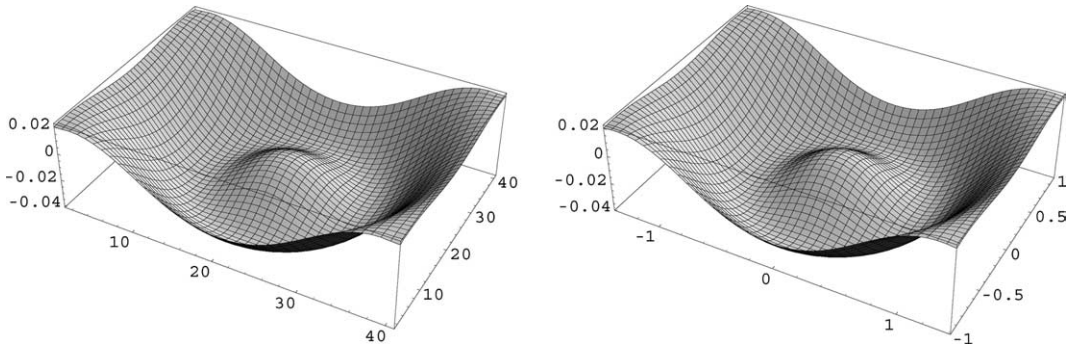

Fig. 11. The right-hand figure is exact solution and the left-hand is numerical solution at time $t = 4$ with $\omega = 2$ and $h = 2/40$, their date come from the right slice plane of Fig. 9.

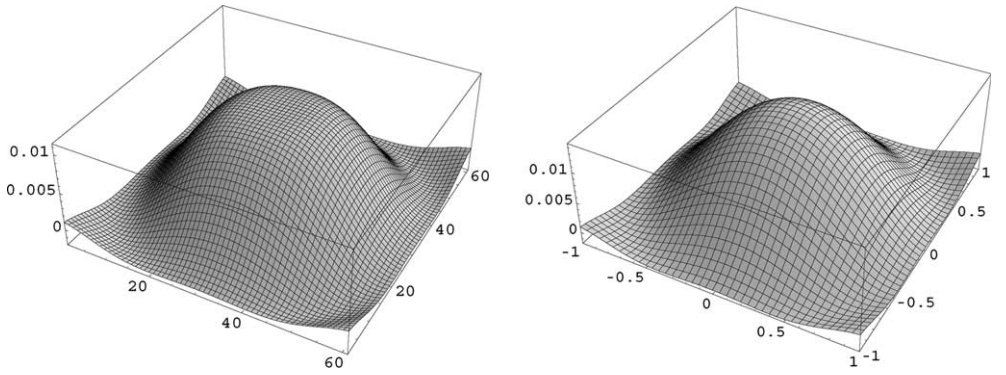

Fig. 12. The right-hand figure is exact solution and the left-hand is numerical solution at time $t = 8$ with $\omega = 3$ and $h = 2/60$, their date come from the left slice plane of Fig. 9.

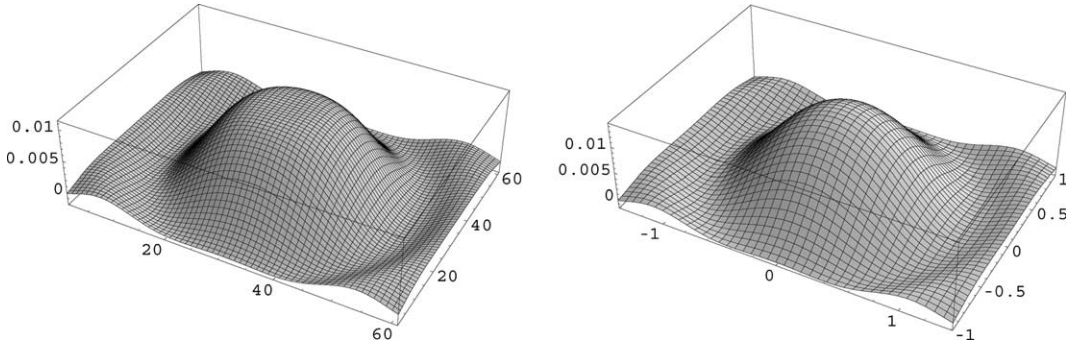

Fig. 13. The right-hand figure is exact solution and the left-hand is numerical solution at time $t = 8$ with $\omega = 3$ and $h = 2/60$, their date come from the right slice plane of Fig. 9.

and the relative L^2-error defined by

$$\|u(\cdot;t) - u_h(\cdot;t)\|_{L^2(\Omega_i)} / \|u(\cdot;t)\|_{L^2(\Omega_i)},$$

where Ω_i is the cubic computational domain and

$$\|v(\cdot;t)\|_{L^2(\Omega_i)} := \left(\sum_j v(\boldsymbol{x}_j;t)^2 h^3 \right)^{1/2}.$$

In the above definition the sum is over all the grid points in the Ω_i. Figs. 14 and 15 show the errors via time t for a frequency $\omega = 4$ with mesh size $h = 10^{-1}, 20^{-1}, 40^{-1}, 80^{-1}$. From the numerical results shown on Figs. 14 and 15 we see that the rate of convergence is one, which coincides with the numerical NRBC, as described in Section 5.2, being first order accurate and that the numerical NRBC with the standard interior non-dissipative scheme is stable.

The above numerical tests were carried out on a Dell PC with PENTIUM III 800 MHz CPU. The actual CPU times required for the computations given in Figs. 14 and 15 ranged from 10 min to hours to a few days. As for the efficiency of the method, we can show theoretically that for M time steps and N points on the cubic boundary $O(MN^2)$ work is required for computing the boundary integral with the discrete for-

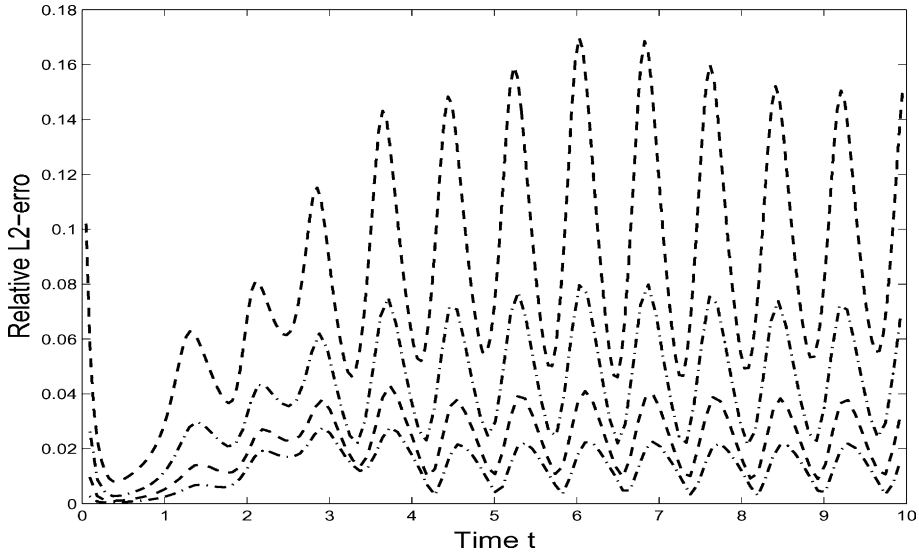

Fig. 14. The relative errors $\|u(\cdot,t)-u_h(\cdot,t)\|_{L^2}/\|u(\cdot,t)\|_{L^2}$ via time t for $\omega=4$, where $h=10^{-1}$, 20^{-1}, 40^{-1}, 80^{-1}.

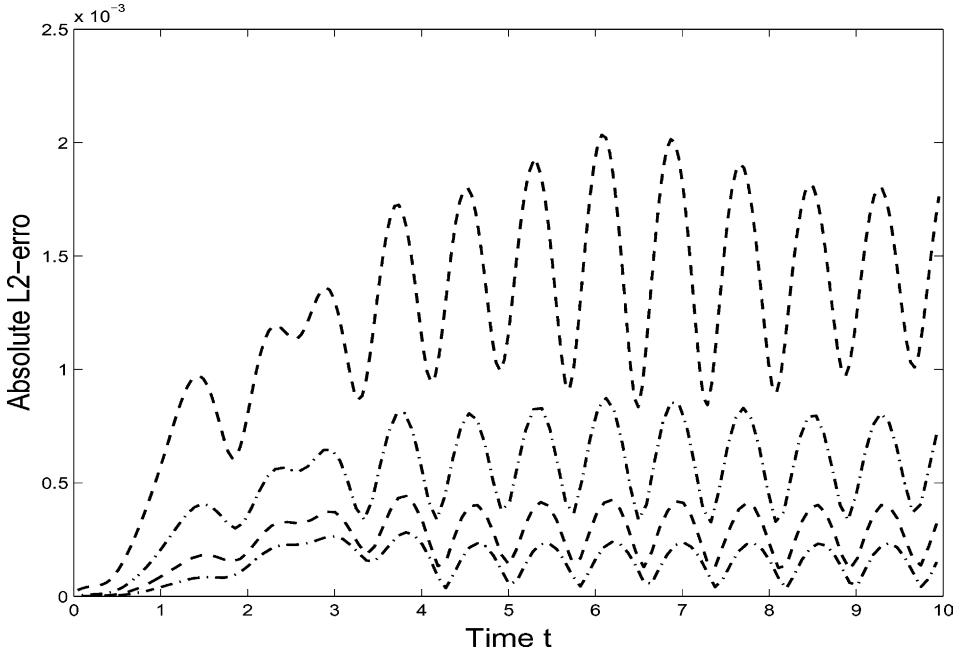

Fig. 15. The absolute errors $\|u(\cdot,t)-u_h(\cdot,t)\|_{L^2}$ via time t for $\omega=4$, where $h=10^{-1}$, 20^{-1}, 40^{-1}, 80^{-1}.

mulae (25)–(30) and $O(MN^{3/2})$ work is required for computing the interior difference scheme (24). In our numerical tests the direct summation of (25)–(30) was used for computing the NRBC, so the operation account was $O(MN^2)$. But we can show that by using a fast graded algorithm ([16]) the amount of work

needed for computing the boundary integral within the same order of accuracy can be reduced to $O(MN^{3/2}\ln N)$, which is about the same order $O(MN^{3/2})$ of the finite-difference calculation used in the interior of the domain. Therefore, the computational cost for the NRBC is acceptable. Since the goal of the present paper is to present a new exact NRBC and to demonstrate its stability and convergency, rather than to try some high order methods and to obtain optimal operation account. The later subjects are important areas of our further research and will be reported elsewhere.

7. Conclusion

In this paper, we have developed, analyzed and tested an exact non-reflecting boundary condition for the numerical simulation of time-dependent wave propagation in unbounded domain. The key ingredient of obtaining the new NRBC is to use the boundary integral equation or modified Kirchhoff formula. The new NRBC eliminates the long-time instability observed in the Ting–Miksis NRBC even if the interior stencil used is non-dissipative scheme and keeps all merits of the original NRBC, such as the extent of temporal non-locality is fixed and limited; no any special function's evaluation is required and the artificial boundary could be any shape. Numerical discretization of the artificial boundary condition on cubic surface is devised and three-dimensional numerical experiments are implemented on the cubic computational domain. Numerical solutions agree very well with the exact solutions and the overall scheme is stable in all our tests.

The new NRBC can also be extended to three dimensional elastodynamics equation, Maxwell equations and so on and those results will be reported elsewhere.

Acknowledgement

The author would like to thank Professors W. Cai, H. Han and T. Tang for bring his attention to this subject and referees for some useful suggestions.

References

[1] B. Alpert, L. Greengard, T. Hagstrom, Nonreflecting boundary conditions for the time-dependent wave equation, J. Comput. Phys. 180 (2002) 270.
[2] B.B. Baker, E.T. Copson, The Mathematical Theory of Huygen's Principle, Oxford University Press, London, 1953.
[3] A. Bayliss, E. Turkel, Radiation boundary conditions for wave-like equations, Commun. Pure Appl. Math. 33 (1980) 707.
[4] B. Engquist, A. Majda, Radiation boundary condition for acoustic and elastic calculations, Commun. Pure Appl. Math. 32 (1979) 313.
[5] K. Feng, Finite element method and natural boundary reduction, in: Proc. of the Int. Congress of Mathematicians, Warsaw, 1983, p. 1439.
[6] D. Givoli, Exact representations on artificial interfaces and applications, Appl. Mech. Rev. 52 (1999) 333.
[7] D. Givoli, Numerical Methods for Problems in Infinite Domains, Elsevier, Amsterdam, 1992.
[8] D. Givoli, D. Cohen, Nonreflecting boundary conditions based on Kirchoff-type formulae, J. Comput. Phys. 117 (1995) 102.
[9] M.J. Grote, J.B. Keller, Exact nonreflecting boundary conditions for the time dependent wave equation, SIAM J. Appl. Math. 55 (1995) 280.
[10] M.J. Grote, J.B. Keller, Nonreflecting boundary conditions for time dependent scattering, J. Comput. Phys. 127 (1996) 52.
[11] D.S. Jones, Acoustic and Electromagnetic Waves, Clarendon Press, Oxford, 1986.
[12] Y. Liu, L. Liu, T. Tang, The numerical computation of connecting orbits in dynamical systems: a rational spectral approach, J. Comput. Phys. 111 (1994) 373.
[13] J.E. Marsden, G.P. Patrick, S. Shkoller, Multi-symplectic geometry, variational integrators and nonlinear PDEs, Commun. Math. Phys. 199 (1999) 351.

[14] V.S. Ryaben'kii, S.V. Tsynkov, V.I. Turchaninov, Global discrete artificial boundary conditions for time-dependent wave propagation, J. Comput. Phys. 174 (2001) 712.
[15] T. Tang, The Hermite spectral method for Gaussian type functions, SIAM J. Sci. Comput. 14 (1993) 594.
[16] T. Tang, Z. Teng, A fast algorithm for computing boundary integrals based on graded mesh, in preparation (2003).
[17] L. Ting, M. Miksis, Exact boundary conditions for scattering problems, J. Acoust. Soc. Am. 80 (1986) 1825.
[18] S.V. Tsynkov, Numerical solution of problems on unbounded domains: a review, Appl. Numer. Math. 27 (1998) 465.
[19] E. Zauderer, Partial Differential Equations of Applied Mathematics, Wiley, New York, 1983.